

Analysis of Spatio-Temporal Changes in Future Artificial Light Pollution and Projections Until 2029 and 2041: A Case Study in the Brazilian States of Roraima, Amazonas, Acre, and Rondônia

Abdulvahap Yılmaz 601

¹Health Services Vocational School, Erzincan Binali Yıldırım University, Erzincan, Türkiye.

Keywords: AL change, remote sensing-GIS, Molusce, Bortle classes

Abstract

This study presents an integrated spatial and temporal analysis of night sky brightness transitions, classified into Bortle classes using the MOLUSCE plugin. Future projections for 2029 and 2041 were generated based on remote sensing data from 2017 and 2020. The results indicate that the "Excellent Sky" and "Typical Dark Sky" classes may decrease by 100% and 56%, respectively, while the "Rural Sky" class could lose approximately 284,679 km². In contrast, the "Rural-suburban Transition" class is projected to grow by 73%, with smaller increases in the "Suburban", "Bright Suburban", "Suburban/urban Transition", and "Urban Center" classes. The "Urban Center" class shows a steady growth rate of 0.004%. These trends suggest a continued spread of light pollution into rural areas. The results provide valuable input for national and local authorities to anticipate future light-pollution patterns and develop effective mitigation strategies.

Resumen

El estudio presenta un enfoque integrado para el análisis temporal y espacial de las transiciones de brillo del cielo nocturno, clasificados en clases de Bortle, utilizando el complemento MOLUSCE. Al combinar datos de teledetección, análisis de cambios en el área y evaluación de la contaminación lumínica, este método produce proyecciones futuras para los años 2029 y 2041 utilizando los conjuntos de datos AL de 2017 y 2020 con la herramienta Molusce. Las tendencias observadas entre 2017 y 2041 muestran que las clases "Cielo excelente" y "Cielo Oscuro Típico" están en riesgo de una disminución del 100% y 56% respectivamente, mientras que se proyecta que la clase "Cielo Rural" perderá aproximadamente 284,679 km². Se espera que la clase "Transición rural-suburbana" aumente en un 73%, mientras que las clases "Suburbana", "Suburbana brillante", "Transición suburbana/urbana" y "Centro urbano" experimenten un aumento relativamente menor. Se observó una tasa de aumento casi constante (0.004%) en la clase "Centro urbano". Estas tendencias evidencian que la contaminación lumínica se está propagando hacia las zonas rurales del área de estudio. Los resultados obtenidos deberían servir de ayuda a las autoridades nacionales y locales para planificar las medidas necesarias mediante la predicción del posible curso futuro de la contaminación lumínica.

1. INTRODUCTION

Artificial light at night (ALAN) is the main cause of light pollution, which is particularly noticeable in urban, industrial, and tourist areas where the human population and economic activities are concentrated. ALAN is known to vary in relation to demographic and economic indicators, such as population (Aksaker et al., 2020) and Gross Domestic Product (GDP) (Yerli et al., 2021). Studies have shown that the areas affected by ALAN are increasing yearly and that light pollution is increasing by 6% annually worldwide (Hölker et al., 2010). Light pollution has significant adverse effects on astronomical observations (Falchi et al., 2011);(Cinzano et al., 2000);(Green et al., 2022); (Varela Perez, 2023); economic activities (Gallaway et al., 2010);(Mitchell

& Gallaway, 2019);(Yılmaz & Özdemir, 2021);(Uchima-Tamayo et al., 2025), ecological systems (Longcore & Rich, 2004); (Hölker et al., 2021);(Hoffmann et al., 2022) and human health (Cho et al., 2015);(Svechkina et al., 2020); (Deprato et al., 2024). It is important to acknowledge and implement preventive measures to reduce the effects of light pollution. Remote sensing methods and Geographic Information System (GIS) infrastructures are widely used for the detection, spatial, and temporal analysis of light pollution (Yılmaz, 2024). Artificial light signals detected remotely at night serve as indicators of the scope of human activities across different times and locations (Chen & Nordhaus, 2011); (Elvidge et al., 2012); (Huang et al., 2014). Day/night images (DNB) acquired with the Visible Infrared Imaging Radiometer (VIIRS)



Figure 1. The political boundaries of Brazil are highlighted by thick red lines on the world map with country boundaries separated by black lines, and the AL map of the study area in 2023. the black areas on the map, created from the VIIRS-DNB dataset (day/night band), represent rural areas with low night sky brightness (light pollution), and the white dots represent the brightness generated at night in areas with high human activity.

provide detailed information on artificial night light caused by human activities with a large radiometric coverage area and high spatial resolution (Miller et al., 2006); (Hillger et al., 2013); (Small et al., 2013); (Elvidge et al., 2013); (Falchi et al., 2016). This information allows remote sensing datasets to represent the same geographic location of a particular pixel over time, so that changes in the environment can be captured (Jiang & Shekhar, 2017), and pixel-level changes can be linked to temporal steps in determining activities and changes that occur within and between years (Roy et al., 2014). For these reasons, the information provided by VIIRS (DNB) thematic layers has great potential for spatiotemporal analyses (Li et al., 2013); (Ma et al., 2014); (Shi et al., 2014); (Jing et al., 2016); (Sharma et al., 2016); (Levin, 2017). This potential can be revealed using GIS infrastructure that focuses on spatial-temporal relationships (Shaw et al., 2016). The Bortle Sky Brightness Classes are a widely used classification system to quantify the effects of artificial light pollution and describe the characteristics of dark skies (Bortle, 2001). These classes can be integrated with regional maps to analyze the impact of light pollution on the environment and provide an important basis for understanding temporal change trends. In this context, the plugin Molusce (Modules for Land Use Change Evaluation), used in the QGIS (Quantum GIS) platform, is an effective tool for analyzing changes between classes, evaluating transition potentials and temporal dynamics of spatial changes, and generating future projections. This plugin predicts spatial shifts by estimating the current state of a pixel based on the initial state, the likelihood of the surrounding neighborhood, and transition laws. It also accurately represents the nonlinear spatial stochastic field change processes and generates complex patterns (Saputra & Lee, 2019). The pixel-based Molusce infrastructure enables temporal and spatial analysis of sky brightness datasets in raster format. In this study, an integrated approach to the temporal and spatial analysis of night sky brightness pixel transitions categorized into Bortle classes using the MOLUSCE plugin is presented. By combining remote sensing data, field change analysis, and light pollution assessment, this method aims to create future forecasts using the Molusce tool. The results obtained will assist national and local authorities in planing measures to address light pollution by predicting its future course.

2. METHODOLOGY

2.1. Study area

When defining the study area, it was important to encompass all levels of the Bortle classification of sky brightness from 2017 to 2023. During the worlwide scan, a region with this characteristic was pinpointed in Brazil. Brazil is the fifth largest country in the world and has a population of more than 203 million (IBGE, 2025)¹. Brazil consists of 26 states and one federal district. The study area was formed by merging the borders of the states of Roraima, Amazonas, Acre, and Rondônia in the north of the country (see map in Figure 1). The populations of the states of Roraima, Amazonas, Acre, and Rondónia are 636 707, 3 941 613, 830 018 and 1 581 196 respectively (IBGE, 2025). The four states cover an area of around 2,321,663 km^2 between the coordinates 5° 17' 7.21" N, 60° 10' 44.48" W and 13° 35' 32.1" S, 60° 39' 22.32" W. Approximately 40% of the world's tropical rainforests are located in the Amazon region (Verweij et al., 2013). Geographically, these states are mainly covered by the Amazon rainforest, the largest tropical rainforest in the world. Astronomically, the geographical location of these states in the Amazon Basin has a negative impact on astronomical studies, as the cloud cover is generally relatively high, and the high humidity negatively affects astronomical transparency (de Sá et al., 2019). However, when suitable atmospheric conditions prevail, forests limit people's freedom of movement and provide an Excellent Sky without artificial light pollution.

2.2. Data Collection

Country and state boundaries were downloaded from GADM (Global Administrative Areas Database²). NTL (Nighttime Lights) data for the years 2017, 2020 and 2023 were downloaded from the Day-Night Band (DNB) dataset of the Visible and Infrared Imaging Suite (VIIRS) of JPSS satellites hosted by the Earth Observation Group (EOG)³. The process steps of the methodological framework shown in Figure 2, which we will discuss in more detail in the following sections, were followed.

2.3. Data management

The VIIRS DNB, Defense Meteorological Satellite Program (DMSP), measures the radiation of the upper atmosphere in the

 $^{^{1}} https://biblioteca.ibge.gov.br/index.php/biblioteca-catalogo?view=detalhes\&id=2102110$

²https://gadm.org/

³https://eogdata.mines.edu/products/vnl/

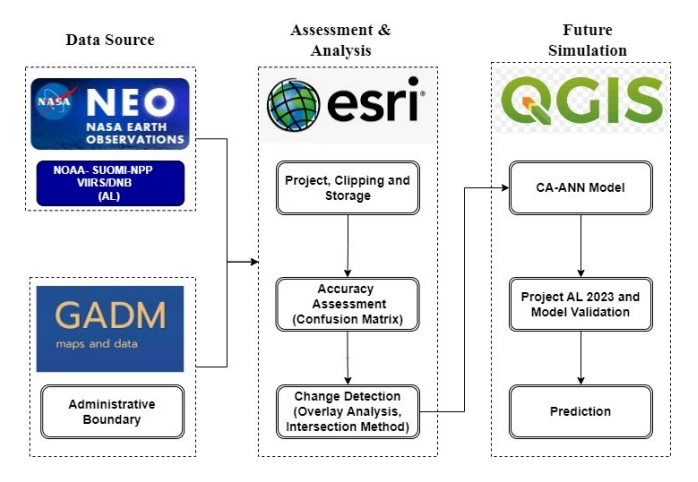


Figure 2. Diagram of the methodical workflow.

wavelength range of 0.5-0.9 μ m between the visible and nearinfrared light spectrum during the night. This measurement was made at a wavelength of about 0.7 μ m and a spatial resolution of 750 m (Schueler et al., 2002). VIIRS DNB radiation measurements have a high calibration accuracy, and the calibration uncertainties reported for Suomi NPP VIIRS DNB are between 2% and 6% (Chen et al., 2017). The NPP-VIIRS DNB data were obtained by regular scans worldwide at approximately 01:30 and 13:30. NPP-VIIRS DNB offers higher radiometric accuracy thanks to its onboard calibration and has a dynamic range of $3.10^{-9} \, nW \, cm^{-2} sr^{-1}$ to $0.02 \ nW cm^{-2} sr^{-1}$, which enables the detection of very small amounts of light (Liao et al., 2013). This feature allows for the detailed mapping of artificial light sources (Falchi et al., 2016). This capability is crucial for determining the ideal regions for astronomical studies by identifying areas with minimal light pollution. The VIIRS cloud mask dataset in GEOTIFF format and with the extension "vcm-orm-ntl" was used in this study, based on the version by Elvidge et al. (2021), where non-artificial light sources were filtered, outliers removed, and night lights included. Data below the VIIRS DNB detection limit of $3 \, nW \, cm^{-2} sr^{-1}$ (Liao et al., 2013) are considered noise and have been filtered out based on this threshold prior to analysis. The unit change was made using equation (1) so that the VIIRS thematic strata could be arranged according to the Bortle scale.

$$SQM = 20.0 - 1.9 \log(AL)$$
 (1)

It was converted to MPSAS (magnitude per square arcsecond) using equation (1) . The study area boundaries were cropped using the ArcGIS 10.8 infrastructure after data collection and assigned to the WGS 1984 projection.

2.4. AL Bortle classification

The Bortle scale is a numerical rating system used to evaluate the brightness of the night sky from an observation point. This scale was developed to measure the ability to observe celestial bodies and the effects of light pollution on such observations. This scale, developed by John E. Bortle and released in 2002, provides a range of categories starting from level 1, denoting the darkest sky, to level 9, indicating the brightest sky. As shown in Table 1, each level is different from the others. In addition, it should not be forgotten that each 5 $Mag/Arcsec^2$ decrease in the SQM value reduces the detectability of the sky brightness by a factor of 100. After the survey and projection of the study area, we classified the AL



Figure 3. Validation diagram between the actual 2023 and the predicted 2023 AL map.

data into eight categories using the ArcGIS 10.8 classification tool according to the Bortle scale (Bortle, 2001): Excellent Sky, Typical Dark sky, Rural Sky, Rural/suburban Transition, Suburban, Bright Suburban, Suburban/urban Transition, and Urban Center (see Table 1). This classification aims to prepare the AL data for modeling and estimating transition potential.

2.5. Analysis of the changes and modeling of the transition potential

We used the land use change simulation mode (MOLUSCE) in QGIS, to estimate the spatial and temporal changes. We calculated the transitions between AL classes during the study periods (2017-2020) and 2017-2023) and generated change maps. The matrix of area change and transition probability was created using AL data and context factors, including the rows and columns of landscape categories in the start and end years. An artificial neural network (ANN) multi-layer perceptron approach was used to model the transition potential.

2.6. Prediction and model validation

In line with numerous studies, the cellular automata-artificial neural networks (CS-ANN) technique was chosen for modeling transition potentials and predicting future scenarios (El-Tantawi et al., 2019). The MOLUSCE plugin is able to efficiently analyze $\,$ the changes that occur on the maps over time (Muhammad et al., 2022). Moreover, it is very effective in terms of assessing AL changes, estimating transition expectations resulting from change analysis, and simulating future scenarios. To determine the reliability of the model used and the prediction results, the MOLUSCE plugin provided a comparison of the real and predicted AL images using a kappa validation technique. To compare the predicted and actual AL for 2023, we calculated the predicted AL for 2023 using the AL datasets and transition matrices from 2017–2020. In the artificial neural network learning process, the AL for 2023 was predicted with 100 iterations and 3×3 pixel neighborhood value, 0.001 learning rate, 10 hidden layers, and 0.05 momentum. Figure 3 shows the validation diagram comparing the actual and predicted artificial light distributions for 2023. After obtaining satisfactory model validation results, the AL for 2029 was projected using the AL datasets from 2017 and 2023, and the AL for 2041 was projected using the AL datasets from 2017 and 2029. The kappa coefficient was calculated using the following formulas (Ullah et al., 2019);(Alawamy et al., 2020); (Satya et al., 2020).

$$kappa = \frac{p_0 - p_e}{1 - p_e} \tag{2}$$

⁴The first class represents Excellent Sky visibility, and the ninth class represents a sky that has been destroyed by the background brightness caused by artificial light pollution.

Color	Bortle	Sky Brightness	Sky Class
Magnitude	Class	magnitude/arcsec²	
Black	1	>21.9	Excellent Sky
Dark gray	2	21.9-21.5	Typical Dark Sky
Blue	3	21.5-21.3	Rural Sky
Green	4	21.3-20.8	Rural/suburban Transition
Yellow	4,5	20.8-20.1	Suburban
Orange	5	20.1-19.1	Bright Suburban
Red	6,7	19.1-18	Suburban/urban Transition
No color	8,9	<18	Urban center

Table 1. Bortle scale and dark sky brightness values.⁴

Where p_0 is the ratio of actual matches, and p_e is the ratio of expected matches.

$$p_0 = \sum_{i=1}^{c} p_{ij} \tag{3}$$

$$p_e = \sum_{i=1}^{c} p_i T \cdot p T_j \tag{4}$$

Here, p_{ij} represents the i-th and j-th cells in the contingency table, $p_i T$ denotes the sum of all cells in the i-th row, pT_j refers to the sum of all cells in the j-th column, and c indicates the number of raster categories. The contingency table is utilized as a matrix representing the frequency distribution of variables and is assessed in this study to reveal the relationship between the i-th and j-th cells. This matrix facilitates the calculation and organization of the interactions within each cell. The results obtained provide an explanation of how well each cell aligns with specific criteria.

2.7. Analysis of the annual rate of change

To calculate the annual rate of change for each Bortle class, the difference between the final and initial years, representing the magnitude of change over the corresponding years, was divided by the initial year and time period. Equation (5) was used to analyze the spatial and temporal magnitude and rate of change in the AL classes.

$$ARC(\%) = \frac{F_y - l_y}{l_y.t} \times 100$$
 (5)

ARC is the annual rate of change of AL classes; l_y and F_y are the fields of the initial and final years, respectively; and t is the time interval.

3. RESULTS AND DISCUSSIONS

3.1. Analysis of the spatio-temporal change

The AL maps, area statistics, and annual rates of change are shown in Table 2. During the study period (2017-2023), we observed an irregular change in AL due to anthropogenic influences (see Figure 4), especially the Rural/suburban transition showed a continuous increase from 358,360.68 km^2 to 2,011,280.85 km^2 , Suburban an increase from 10,651.98 km^2 to 27,796.48 km^2 , Bright Suburban an increase from 3,938.05 km^2 to 6,516.86 km^2 , suburban/urban transition an increase from 1,521.77 km^2 to 2,092.19 km^2 , Urban Center an increase from 1,240.65 km^2 to 1,372.55 km^2 . In contrast, there was a linear decrease from 108,934.61 km^2 to 8.71 km^2 for an Excellent Sky. Similarly, there was a decrease from 1,315,797.1 km^2 to 2,489.65 km^2 for Typical

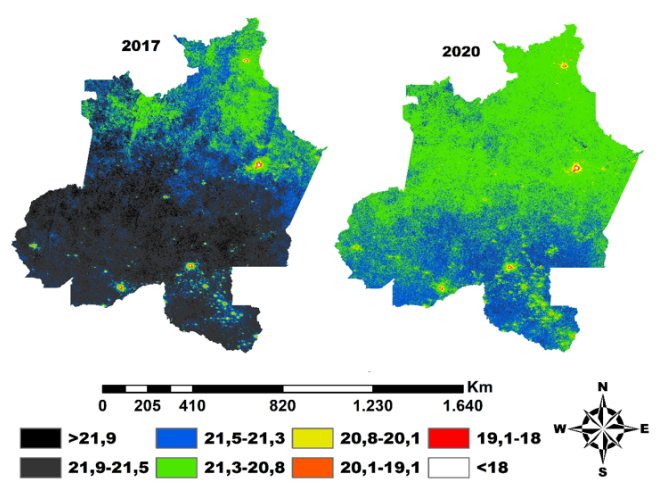


Figure 4. AL maps colored by Bortle classes for 2017 and 2020. Black shades represent Excellent Sky and Typical Dark sky classes with low human activity, while white represents the Urban Center class with high human activity.

Dark sky values and from $521,102.75 \ km^2$ to $270,105.78 \ km^2$ for Rural Sky values. All classes of sky showed similar increases and decreases between 2017 and 2020 as between 2017 and 2023 (Table 2).

Table 2 presents the spatiotemporal extent across all AL classes and the annual percentage change between 2017 and 2023. The AL change analysis aims to show the spatial dynamic changes in the AL pattern over the analyzed period (see Figure 5). The analysis results from 2017 to 2023 show a dramatic decline in the "Excellent Sky" and "Typical Dark Sky" classes. The areas of these classes shrank, on average, by 16.67% and 16.64% per year, respectively. The "Rural Sky" class is shrinking at an average annual rate of approximately 8.03%. In contrast, the most dramatic increase was observed in the "Rural/Suburban Transition" class, which is growing at an average annual rate of 76.87% (see Table 2). In addition, the "Suburban", "Bright Suburban", and "Suburban/urban Transition" classes increased by 26.83%, 10.91%, and 6.25% per year, respectively. The "Urban center" class showed a smaller change compared to the other rising classes, with an annual increase of approximately 1.8%. The total area of the study border shown in Table 2 is the sum of the light intensity emanating from the surface (divided into Bortle classes). The fluctuations in the light intensity filtered as noise (below 3 $nWcm^{-2}sr^{-1}$) per year led to negligible differences in

Sky Brightness								
Mag/Arcsec ²	2017		2020		2023		ARC %	ARC %
	km^2	%	km^2	%	km^2	%	2017-2020	2017-2023
>21.9	108934.61	4.69	240.74	0.01	8.71	0.0004	-33.26%	-16.67%
21.9-21.5	1315797.10	56.68	62263.58	2.68	2489.65	0.1072	-31.76%	-16.64%
21.5-21.3	521102.75	22.45	772380.01	33.27	270105.78	11.6342	16.07%	-8.03%
21.3-20.8	358360.68	15.44	1461596.10	62.96	2011280.85	86.6310	102.62%	76.87%
20.8-20.1	10651.99	0.46	17185.96	0.74	27796.48	1.1973	20.45%	26.83%
20.1-19.1	3938.06	0.17	4887.50	0.21	6516.86	0.2807	8.04%	10.91%
19.1-18	1521.77	0.07	1713.67	0.07	2092.19	0.0901	4.20%	6.25%
<18	1240.65	0.05	1228.84	0.05	1372.55	0.0591	-0.32%	1.77%
Total	2,321,548		2,321,496		2,321,663			

Table 2. Area sizes (km^2) and annual rate of change (ARC) of AL classes between 2017 and 2023.

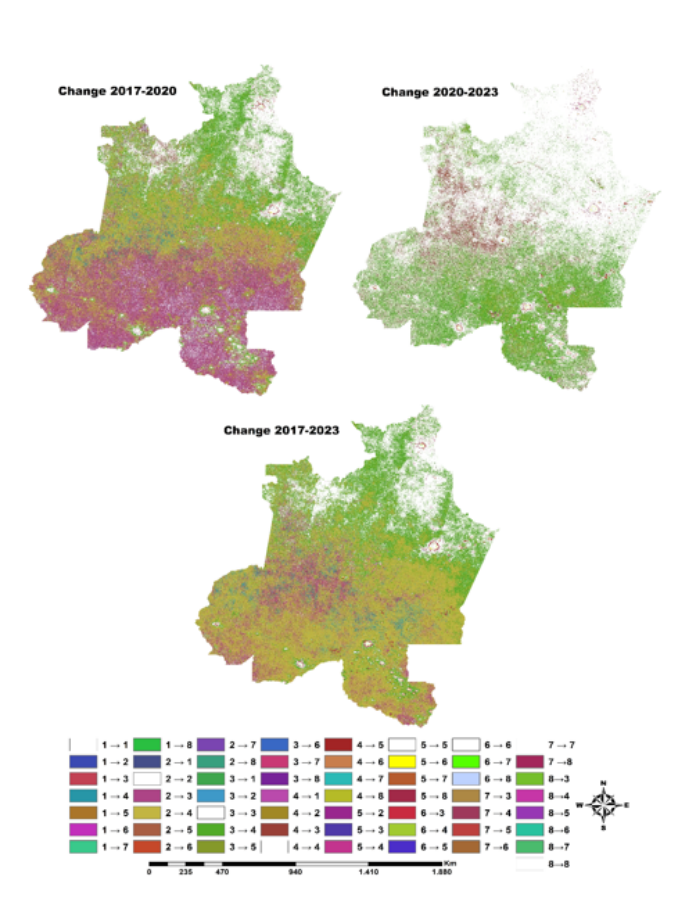


Figure 5. Colored AL change maps 2017–2020, 2017-2023, 2020-2023. Colors other than white highlight the transition from one class to another. The white color represents unchanged classes. 1: Excellent Sky, 2: Typical Dark Sky, 3: Rural Sky, 4: Rural/suburban Transition, 5: Suburban, 6: Bright Suburban, 7: Suburban/urban Transition, 8: Urban Center classes.

the total area, as shown in Table 2. The changes in the AL classes between 2017-2020 and 2020-2023 are shown in Table 3. Table 3 shows the areas gained and lost for each brightness class in the time intervals used in this study.

3.2. AL transition analysis

The transition matrix is an important part of the analysis of temporal changes between AL classes. The matrix represents the pixel ratios that change from one Bortle class to another. The columns of the transition matrix table represent the Bortle classes in the initial year, whereas the rows show the Bortle classes in the final year in the same order. The entries outside the diagonal represent the transition dimension from one class to another, whereas the diagonal entries represent the stability dimension of the respective class. The closer the values of the diagonal entries are to 1, the higher the stability of the Bortle class is. Transition matrices are used to analyze the transitions between different classes (Xiao et al., 2022). In our study area, the transition potential matrices for the time intervals 2017-2020, 2020-2023, and 2017-2023 were calculated using QGIS/MOLUSCE based on the available AL data. These matrices were used to create transition maps of the classes (see Figure 5). The transition potential matrix for the period 2017-2020 is shown in Table 4. Rural/suburban transition and Urban Center are the most stable brightness classes with probabilities of 0.903 and 0.88, respectively, and contribute to the Rural Sky with transition values of 0.07 and 0.003, respectively. The least stable brightness classes are the Excellent Sky and Typical Dark sky classes with values of 0.000087 and 0.047442, respectively. The transition potential matrix for the year 2020-2023 is shown in Table 5. The most stable brightness classes are Urban Centers and Rural/suburban areas, with probabilities of 0.91 and 0.9, respectively. The least stable brightness classes are Typical Dark Sky and Excellent Sky, with values of 0.001 and 0.002, respectively, as in 2017-2020.

Additionally, the AL dataset for the period 2017-2023 is used along with the transition probability matrix for the 2029 projection. According to the transition matrix for the period between 2017 and 2023 (Table 6), the Rural/suburban transition class was found to be stable with a value of 0.94, while the Excellent Sky, Typical Dark Sky, Rural Sky, and Bright Suburban classes exhibited instability values of 0.000004, 0.0006, 0.057, and 0.62, respectively. The Rural Suburban transition class will experience more stable phenomena between 2017 and 2029 than the other classes (Table 7).

3.3. Modeling the transition potential and model validation

The MOLUSCE plugin can use transition potential modeling, such as multi-criteria evaluation, ANN (multi-layer perceptron), evidence weights, CA algorithm, and logistic regression, to generate future simulations (Chisanga et al., 2024); (Vaddiraju et al., 2023). In this study, the CA-ANN approach was used

Table 3. Temporal changes 2017–2023

Sky Brightness				
Mag/Arcsec ²	2017-2020		2020-2023	
	km^2	%	km^2	%
>21.9	-108693.9	-4.68	-232.04	-0.01
21.9-21.5	-1253533.5	-54.00	-59773.94	-2.57
21.5-21.3	251277.3	10.82	-502274.23	-21.64
21.3-20.8	1103235.4	47.52	549684.75	23.67
20.8-20.1	6534.0	0.28	10610.52	0.46
20.1-19.1	949.4	0.04	1629.36	0.07
19.1-18	191.9	0.01	378.52	0.02
<18	-11.8	0.00	143.72	0.01

Table 4. Transition matrix from 2017-2020

Year					2020				
2017	Sky Brightness Mag/Arcsec ²	>21.9	21.9-21.5	21.5-21.3	21.3-20.8	20.8-20.1	20.1-19.1	19.1-18	<18
	>21.9	0.000087	0.050435	0.427833	0.520099	0.001053	0.000379	0.000094	0.000020
	21.9-21.5	0.000069	0.047442	0.469636	0.480940	0.001445	0.000374	0.000080	0.000013
	21.5-21.3	0.000161	0.010035	0.165911	0.821502	0.001947	0.000362	0.000071	0.000011
	21.3-20.8	0.000157	0.004734	0.071623	0.903020	0.019036	0.001131	0.000265	0.000035
	20.8-20.1	0.000040	0.003601	0.035088	0.177796	0.689194	0.091463	0.002575	0.000241
	20.1-19.1	0.000000	0.002912	0.030326	0.093946	0.140369	0.666081	0.065707	0.000659
	19.1-18	0.000000	0.002733	0.021004	0.036973	0.011797	0.161703	0.705654	0.060135
	<18	0.000000	0.000528	0.003343	0.006687	0.001760	0.000880	0.101707	0.885096

Table 5. Transition matrix from 2020–2023

Year				2023					
2020	Sky Brightness Mag/Arcsec ²	>21.9	21.9-21.5	21.5-21.3	21.3-20.8	20.8-20.1	20.1-19.1	19.1-18	<18
	>21.9	0.00278	0.02317	0.123262	0.848007	0.00278	0.00000	0.00000	0.00000
	21.9-21.5	0.000024	0.001022	0.152431	0.839886	0.005047	0.001199	0.000305	0.000085
	21.5-21.3	0.000002	0.000775	0.160584	0.831997	0.005177	0.001119	0.000279	0.000067
	21.3-20.8	0.000003	0.001208	0.089655	0.900447	0.007925	0.000605	0.000136	0.000021
	20.8-20.1	0.000012	0.000062	0.009381	0.263837	0.652619	0.07231	0.001531	0.000247
	20.1-19.1	0.00000	0.000044	0.006883	0.178526	0.098864	0.649174	0.065062	0.001447
	19.1-18	0.00000	0.00000	0.002909	0.113964	0.020238	0.079433	0.702884	0.080572
	<18	0.00000	0.00000	0.002837	0.025887	0.001596	0.00000	0.059043	0.910638

to forecast the future and model the transition potential. To predict the thematic AL layer for 2023, the AL shift maps for 2017-2020 were used, and a kappa value of 0.83 was obtained. After generating the predicted 2023 thematic AL layer for the study area, it was compared with the actual 2023 thematic AL layer (see Figure 3). The comparison yielded an overall accuracy of 62.77% and an overall kappa value of 0.42. Figure 6 and Table 8 present the predicted and actual AL maps and their associated statistics for 2023.

3.4. Estimation of AL

After obtaining satisfactory results from model validation, we estimated the AL for 2029 and 2041. Using the AL dataset for 2017 and 2023 and the transition probability matrix (Table 6), the AL for 2029 was estimated, and a kappa value of 0.72 was obtained. In addition, the AL dataset for 2017 and 2029, including the transition matrix (Table 7), was used to predict the year 2041,

⁵Accuracy:62.77, Kappa ANN: 0.83, Value Validation: 0.42

Table 6. Transition matrix from 2017-2023

Year				2023					
2017	Sky Brightness Mag/Arcsec ²	>21.9	21.9-21.5	21.5-21.3	21.3-20.8	20.8-20.1	20.1-19.1	19.1-18	<18
	>21.9	0.000004	0.000876	0.131226	0.866268	0.001270	0.000249	0.000089	0.000018
	21.9-21.5	0.000003	0.000663	0.160876	0.834544	0.003107	0.000610	0.000156	0.000041
	21.5-21.3	0.000003	0.000610	0.057507	0.937517	0.003858	0.000414	0.000081	0.000009
	21.3-20.8	0.000001	0.000205	0.017923	0.949225	0.031425	0.001054	0.000145	0.000022
	20.8-20.1	0.000000	0.000020	0.005533	0.189667	0.653059	0.147999	0.003561	0.000161
	20.1-19.1	0.000000	0.000000	0.006098	0.120262	0.142787	0.626140	0.101857	0.002857
	19.1-18	0.000000	0.000000	0.007913	0.050065	0.036542	0.130341	0.668968	0.106172
	<18	0.000000	0.000000	0.000528	0.008974	0.003695	0.000704	0.107338	0.878761

Table 7. Transition matrix from 2017-2029

Year				2029					
2017	Sky Brightness Mag/Arcsec ²	>21.9	21.9-21.5	21.5-21.3	21.3-20.8	20.8-20.1	20.1-19.1	19.1-18	<18
	>21.9	0.000009	0.002622	0.202718	0.789502	0.004044	0.000795	0.000255	0.000056
	21.9-21.5	0.000004	0.001223	0.161069	0.831052	0.005308	0.001031	0.000253	0.000059
	21.5-21.3	0.000004	0.000798	0.052535	0.942150	0.003958	0.000453	0.000092	0.000010
	21.3-20.8	0.000001	0.000316	0.016344	0.951555	0.030524	0.001088	0.000151	0.000022
	20.8-20.1	0.000000	0.000020	0.005110	0.190451	0.649538	0.151178	0.003561	0.000141
	20.1-19.1	0.000000	0.000000	0.005824	0.120097	0.121470	0.646358	0.103395	0.002857
	19.1-18	0.000000	0.000000	0.007049	0.050784	0.013667	0.143576	0.678464	0.106460
	<18	0.000000	0.000000	0.000352	0.009150	0.002815	0.001056	0.107690	0.878937

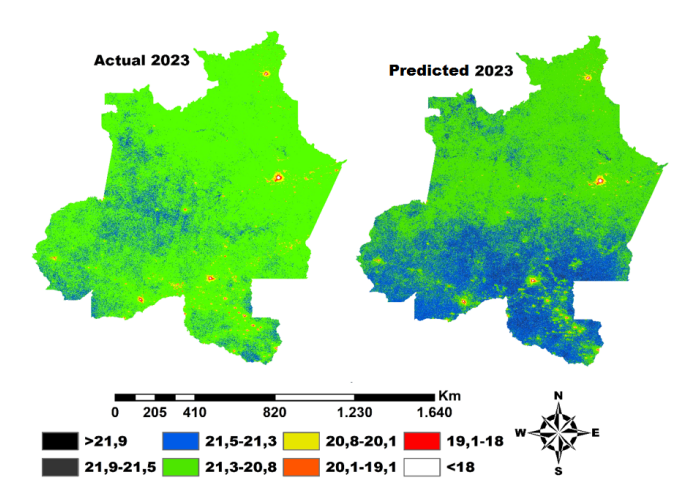


Figure 6. Actual and predicted AL maps colored by Bortle classes for 2023. Black shades represent excellent skies and Typical Dark sky classes with low human activity, while the color white represents the Urban Center class with high human activity.

and a kappa value of 0.91 was obtained. The projected AL map, field statistics, and kappa values for the general validity for 2029 and 2041 are shown in Figure 7 and Table 9.

Table 8. Actual and predicted classified AL statistics for 2023 5

Sky Brightness	Actual		Predic	ted
Mag/Arcsec ²	km^2	%	km^2	%
>21.9	8.71	0.0004	173.12	0.007
21.9-21.5	2489.65	0.1072	55734.768	2.401
21.5-21.3	270105.78	11.6350	766027.43	32.997
21.3-20.8	2011280.85	86.6373	1473528.2	63.473
20.8-20.1	27796.48	1.1974	19148.735	0.825
20.1-19.1	6516.86	0.2807	4162.4819	0.179
19.1-18	2092.19	0.0901	1544.3935	0.067
<18	1372.55	0.0591	1177.331	0.051

3.5. Change between 2017 and 2041

The AL change analysis aims to show the spatial dynamic changes in the AL pattern during the study period. According to the results obtained for the period from 2017 to 2041, the Excellent Sky class experienced a loss of $108,929\ km^2$. While it accounted for approximately 5% of the total surface area in 2017, it nearly disappeared by 2041. The Typical Dark sky class experienced the most dramatic loss, with an area loss of $1,314,649\ km^2$ This represents a loss of approximately 56% between the years studied. The Rural Sky class lost $284,679\ km^2$ of area, which corresponds to approximately 12% of the total area. The rural-suburban transition

⁶Kappa(2029): 0.72, Kappa(2041): 0.91

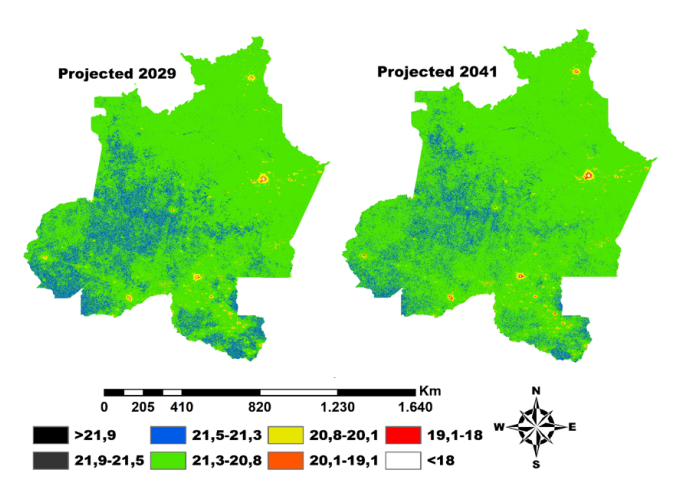


Figure 7. Projected AL maps for 2029 and 2041, colored by Bortle classes. Black shades represent the Excellent Sky and Typical Dark sky classes with low human activity, while white represents the Urban Center class with high human activity.

Table 9. Projected AL classes for the 2029 and 2041 field statistics⁶

Sky Brightness	2029		2041	
$Mag/Arcsec^2$	km^2	%	km^2	%
>21.9	3.84	0.00	5.99	0.00
21.9-21.5	908.09	0.04	1147.88	0.05
21.5-21.3	361314.31	15.56	236423.52	10.18
21.3-20.8	1925811.85	82.95	2051122.53	88.35
20.8-20.1	27387.13	1.18	24190.64	1.04
20.1-19.1	3622.44	0.16	5505.09	0.24
19.1-18	1639.88	0.07	1884.97	0.08
<18	918.80	0.04	1325.71	0.06

Table 10. Estimated temporal changes between 2023 and 2041

Sky Brightness	2023-2029		2029-20	041
$Mag/Arcsec^2$	km^2	%	km^2	%
>21.9	-4.87	0.00	2.15	0.00
21.9-21.5	-1581.56	-0.07	239.79	0.01
21.5-21.3	91208.53	3.93	-124890.8	-5.38
21.3-20.8	-85469	-3.68	125310.7	5.40
20.8-20.1	-409.35	-0.02	-3196.49	-0.14
20.1-19.1	-2894.42	-0.12	1882.65	0.08
19.1-18	-452.31	-0.02	245.09	0.01
<18	-453.75	-0.02	406.91	0.02

class showed the most dramatic increase. A 73% growth was achieved across the entire area, with an increase in the area of $1,692,762\ km^2$. The suburban class increased by $13,538\ km^2$, which corresponds to approximately 0.6% of the total area. The classes "Bright Suburban area", "suburban/urban transition" and "Urban Center" do not show significant increases, and increases of 0.07%, 0.01%, and 0.004% of the total area were found, respectively. The spatial changes owing to class transitions during the analyzed periods are shown in Figure 8.

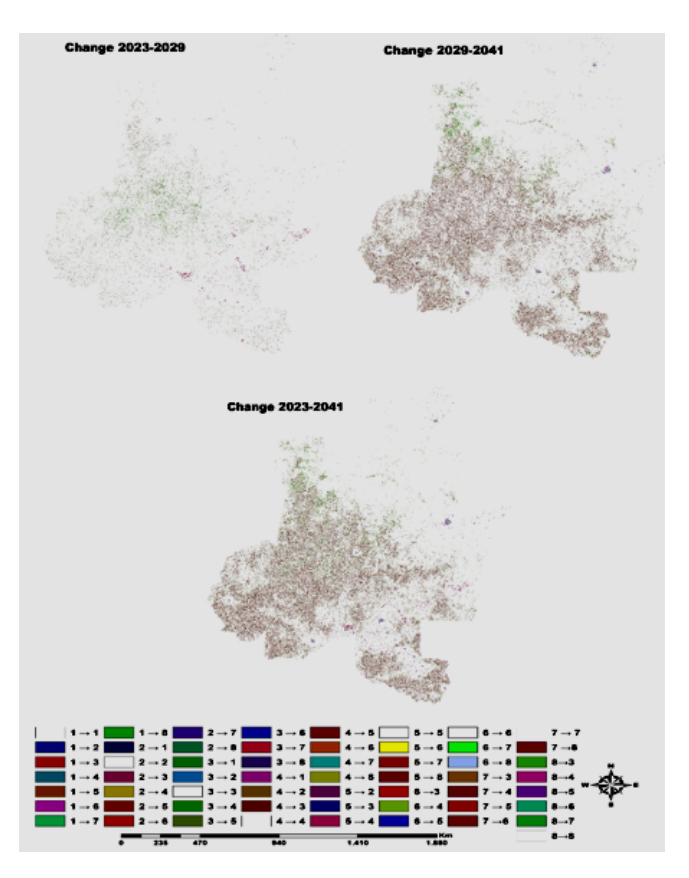


Figure 8. Colored maps of estimated AL changes 2023–2029, 2029-2041, 2023-2041. Colors other than white highlight the transition from one class to another. White colors represent unchanged classes. 1: Excellent Sky, 2: Typical Dark Sky, 3: Rural Sky, 4: Rural/suburban transition, 5: Suburban, 6: Bright Suburban, 7: Suburban/urban Transition, 8: Urban Center classes are shown.

4. Discussion

In this study, the temporal and spatial dynamic changes in artificial light patterns between 2017 and 2041 were analyzed using remote sensing data and GIS within an area encompassing the Brazilian states of Roraima, Amazonas, Acre, and Rondônia, based on the Bortle classification. The results of the analysis show that the impact of light pollution in the region has increased dramatically over the years, leading to significant losses in the dark sky classes. The observed trends suggest that the natural classes, particularly "Excellent Sky" and "Typical Dark Sky", are likely to face near-complete depletion in the future, with predicted losses reaching approximately 100% and 56%, respectively, if current environmental pressures persist. Similarly, the Rural Sky class is anticipated to experience significant reductions, potentially losing even more land beyond the already displaced 284,679 km^2 , underscoring the urgency for sustainable intervention. The "Rural-suburban transition" class is expected to experience the largest increase, with projections suggesting a 73% rise. This trend will likely signify a gradual transformation of rural areas into semi-urban zones, leading to the continued spread of light pollution in rural regions. A relatively smaller increase was observed in the Suburban, Bright Suburban, Suburban/Urban Transition, and Urban Center classes. The fact that the change in the Urban Center class was only 0.004% shows that these classes already have a high level of light pollution and that the growth is concentrated in rural areas with low light pollution. This result can be linked to the fact that the study area consists of forested areas that are not suitable for urbanization. These results show that the rapid increase in artificial light, especially in large and relatively sparsely populated regions such as Roraima, Amazonas, Acre, and Rondônia, poses a serious threat to the protection of natural areas. Apart from the negative effects of this rapid increase in light pollution on astronomical studies, the ecological consequences should also be discussed by experts in this field. In this context, the spatial analysis results emphasize the urgency of implementing measures to manage and protect against light pollution. In these regions of Brazil, sustainable lighting technologies and strategies for protecting natural areas are necessary. Curbing the increasing trends, especially in rural areas, will contribute to the protection of dark skies and environmental sustainability. This study, conducted using the VIIRS/DNB dataset and the Bortle classification, provides an important scientific basis for understanding the spatial changes caused by artificial light pollution and how to tackle this problem. Such analyses can be used more effectively for light pollution management and policy-making processes.

5. Conclusions and recommendations

The VIIRS/DNB NTL data were categorized according to the Bortle classification, and projections of light pollution for 2029 and 2041 were generated using the QGIS/MOLUSCE plugin for the study area, which includes the Brazilian states of Roraima, Amazonas, Acre, and Rondônia. The integration of VIIRS/DNB data with the Bortle classification and its analysis using QGIS/MOLUSCE can significantly increase the sensitivity of spatial analyses. This study provides valuable insights that can form the basis for developing future light pollution management strategies. It has been shown that specific strategies need to be developed for the protection of classes such as "Excellent Sky" and "Typical Dark Sky". In this context, the protection of nature reserves, the creation of light pollution management plans, and the reinforcement of environmental awareness campaigns can be proposed. Furthermore, it was found that this comprehensive method, applied for the first time in this study, increased the sensitivity of spatial analysis and strengthened the reliability of future projections. The inclusion of variables such as GDP and population, which affect light pollution, can further increase the accuracy and effectiveness of the analyses. Such inclusion will contribute to the development of more comprehensive and realistic measures to combat the effects of light pollution.

6. CONCLUSION

- This study is the first to present a project-based modeling of light pollution and future projections of light pollution using QGIS/MOLUSCE by combining VIIRS/DNB data with Bortle classification.
- Light pollution is increasing rapidly in the Amazon rainforest region. The future of dark-sky classes is under threat. The Excellent Sky class is expected to almost disappear, and the Typical Dark sky class will also decline rapidly.
- The "Excellent Sky" class lost 108,929 km² of land in the period 2017–2041. While it accounted for 5% of the total area in 2017, it is expected to almost disappear by 2041.
- The "Typical Dark Sky" class is expected to be the class with the largest decline, losing 1,314,649 km² of area. This corresponds to approximately 56 % of the total area. A significant decline is also predicted for the "Rural Sky" class:

- 284,679 km^2 will be lost, which corresponds to a decline of approximately 12 %.
- The "Rural-suburban transition" class recorded the largest increase with an area of $1,692,762 \, km^2$, which corresponds to an overall growth of 73 %. This indicates that rural areas are transforming into semi-urban areas.

■ REFERENCES

Aksaker, N. A. Z. I. M., Yerli, S. K., Kurt, Z., et al. 2020, Ap&SS, 365, 153, doi: 10.1007/s10509-020-03815-9

Alawamy, J. S., Balasundram, S. K., Hanif, A. H. M., & Sung, C. T. B. 2020, Sust, 12, 4490, doi: 10.3390/su12114490

Bortle, J. E. 2001, S&T, 101, 126

Chen, H., Lei, N., Sun, C., & Xiong, X. 2017, in IGARSS 2017, IEEE, 5398–5401, doi: 10.1109/IGARSS.2017.8128224

Chen, X., & Nordhaus, W. D. 2011, PNAS, 108, 8589, doi: 10.1073/pnas.1017031108

Chisanga, C. B., Phiri, D., & Mubanga, K. H. 2024, Discover Environment, 2, 38, doi: 10.1007/s44274-024-00066-w

Cho, Y., Ryu, S.-H., Lee, B. R., et al. 2015, Chronobiology international, 32, 1294, doi: 10.3109/07420528.2015.1073158

Cinzano, P., Falchi, F., Elvidge, C. D., & Baugh, K. E. 2000, MNRAS, 318, 641, doi: 10.1046/j.1365-8711.2000.03562.x

de Sá, S. S., Rizzo, L. V., Palm, B. B., et al. 2019, Atmospheric Chemistry and Physics, 19, 7973, doi: 10.5194/acp-19-7973-201

Deprato, A., Maidstone, R., Cros, A. P., et al. 2024, BMC medicine, 22, 67, doi: 10.1186/s12916-024-03291-5

El-Tantawi, A. M., Bao, A., Chang, C., & Liu, Y. 2019, EMnAs, 191, 480, doi: 10.1007/s10661-019-7478-0

Elvidge, C., Baugh, K., Zhizhin, M., & Hsu, F.-C. 2013, Proceedings of the Asia-Pacific Advanced Network, 35, 62, doi: 10.7125/APAN.35.7

Elvidge, C. D., Baugh, K., Zhizhin, M., Hsu, F. C., & Ghosh, T. 2021, Remote Sensing of Night-Time Light (Taylor & Francis). https://www.taylorfrancis.com/reader/download/514ebd14-9c12-4c2e-aa2d-0dfef1e4659d/chapter/pdf?context=ubx

Elvidge, C. D., Baugh, K. E., Anderson, S. J., Sutton, P. C., & Ghosh, T. 2012, Social Geography, 7, 23, doi: 10.5194/sg-7-23-2012

Falchi, F., Cinzano, P., Elvidge, C. D., Keith, D. M., & Haim, A. 2011, JEnvM, 92, 2714, doi: 10.1016/j.jenvman.2011.06.029

Falchi, F., Cinzano, P., Duriscoe, D., et al. 2016, SciA, 2, e1600377, doi: 10.1126/sciadv.1600377

Gallaway, T., Olsen, R. N., & Mitchell, D. M. 2010, Ecological Economics, 69, 658, doi: 10.1016/j.ecolecon.2009.10.003

Green, R. F., Luginbuhl, C. B., Wainscoat, R. J., & Duriscoe, D. 2022, A&ARv, 30, 1, doi: 10.1007/s00159-021-00138-3

Hillger, D., Kopp, T., Lee, T., et al. 2013, BAMS, 94, 1019, doi: 10.1 175/BAMS-D-12-00097.1

Hoffmann, J., Hölker, F., & Eccard, J. A. 2022, Frontiers in Ecology and Evolution, 9, 779825, doi: 10.3389/fevo.2021.779825

Hölker, F., Moss, T., Griefahn, B., et al. 2010, EcSoc, 15, 13., doi: 10 .5751/ES-03685-150413

Hölker, F., Bolliger, J., Davies, T. W., et al. 2021, Frontiers in Ecology and Evolution, 9, 767177

Huang, Q., Yang, X., Gao, B., Yang, Y., & Zhao, Y. 2014, RemS, 6, 6844, doi: 10.3390/rs6086844

IBGE. 2025, Pesquisa de Pós-Enumeração do Censo Demográfico 2022: resultados da análise da cobertura (Rio de Janeiro, RJ -Brasil: IBGE). https://biblioteca.ibge.gov.br/index.php/bibliot eca-catalogo?view=detalhes&id=2102110

- Jiang, Z., & Shekhar, S. 2017, Spatial Big Data Science, doi: 10.1 007/978-3-319-60195-3
- Jing, X., Shao, X., Cao, C., Fu, X., & Yan, L. 2016, RemS, 8, 17, doi: 10.3390/rs8010017
- Levin, N. 2017, RSEnv, 193, 150, doi: https://doi.org/10.1016/j.rse. 2017.03.003
- Li, X., Xu, H., Chen, X., & Li, C. 2013, RemS, 5, 3057, doi: 10.339 0/rs5063057
- Liao, L. B., Weiss, S., Mills, S., & Hauss, B. 2013, JGRD, 118, 12705, doi: https://doi.org/10.1002/2013JD020475
- Longcore, T., & Rich, C. 2004, FrEE, 2, 191, doi: https://doi.org/ 10.1890/1540-9295(2004)002[0191:ELP]2.0.CO;2
- Ma, T., Zhou, C., Pei, T., Haynie, S., & Fan, J. 2014, RSL, 5, 165, doi: 10.1080/2150704X.2014.890758
- Miller, S. D., Hawkins, J. D., Kent, J., et al. 2006, BAMS, 87, 433, doi: 10.1175/BAMS-87-4-433
- Mitchell, D., & Gallaway, T. 2019, Tourism Review, 74, 930, doi: 10 .1108/TR-10-2018-0146
- Muhammad, R., Zhang, W., Abbas, Z., Guo, F., & Gwiazdzinski, L. 2022, Land, 11, 419, doi: 10.3390/land11030419
- Roy, D., Wulder, M., Loveland, T., et al. 2014, RSEnv, 2014, 154, doi: 10.1016/j.rse.2014.02.001
- Saputra, M. H., & Lee, H. S. 2019, Sust, 11, doi: 10.3390/su111130
- Satya, B. A., Shashi, M., & Deva, P. 2020, Applied Geomatics, 12, 281, doi: 10.1007/s12518-020-00298-4
- Schueler, C. F., Clement, J. E., Ardanuy, P. E., et al. 2002, in Earth Observing Systems VI, Vol. 4483, SPIE, 11–23, doi: 10.1117/12 .453451

- Sharma, R. C., Tateishi, R., Hara, K., Gharechelou, S., & Iizuka, K. 2016, IJDE, 9, 1004, doi: 10.1080/17538947.2016.1168879
- Shaw, S., Tsou, M., & Ye, X. 2016, IJGIS, 30, 1687, doi: 10.1080/13 658816.2016.1164317
- Shi, K., Huang, C., Yu, B., et al. 2014, RSL, 5, 358, doi: 10.1080/21 50704X.2014.905728
- Small, C., Elvidge, C. D., & Baugh, K. 2013, in Joint Urban Remote Sensing Event (IEEE), 230, doi: 10.1109/JURSE.2013.6550707
- Svechkina, A., Portnov, B. A., & Trop, T. 2020, LaEco, 35, 1725, doi: 10.1007/s10980-020-01053-1
- Uchima-Tamayo, J. P., Angeloni, R., Jaque Arancibia, M., Goez Theran, C., & Rúa Restrepo, J. F. 2025, RMxAA, 61, 123, doi: 10 .22201/ia.01851101p.2025.61.01.10
- Ullah, S., Tahir, A. A., Akbar, T. A., et al. 2019, Sust, 11, 5492, doi: 10.3390/su11195492
- Vaddiraju, S. C., Talari, R., Bhavana, K., & Apsana, S. 2023, EMnAs, 195, 1499, doi: 10.1007/s10661-023-12128-2
- Varela Perez, A. M. 2023, Sci, 380, 1136, doi: 10.1126/science.ad g0269
- Verweij, P., Schouten, M., Van Beukering, P., et al. 2013, WWF-Netherlands Report
- Xiao, J., Watanabe, T., Lu, X., et al. 2022, PCE, 126, 103041, doi: 10 .1016/j.pce.2021.103041
- Yerli, S. K., Aksaker, N., Bayazit, M., et al. 2021, Ap&SS, 366, 34, doi: 10.1007/s10509-021-03942-6
- Yılmaz, A. 2024, TJAA, 5, 22, doi: 10.55064/tjaa.1449416
- Yılmaz, A., & Özdemir, T. 2021, TJAA, 2, 38